Coulomb drag between quantum wires: A nonequilibrium many-body approach

Chenyi Zhou and Hong Guo
Center for the Physics of Materials, Department of Physics, McGill University, Montreal, H3A 2T8, Canada

(Received 24 July 2018; revised manuscript received 13 December 2018; published 14 January 2019)

We present a real-space theoretical formalism and its numerical implementation for investigating nonequilibrium quantum Coulomb drag between parallel two-terminal transport structures in quasi-one-dimension. In addition to the Coulomb interaction and the finite external potential bias, our formalism takes into account the effects of impurity disorder. The theory is formulated in the nonequilibrium Green's function formalism, with the long-range Coulomb interaction treated at the many-body GW approximation level and the disorder-average carried out at the coherent potential approximation (CPA) level. The coupled GW and CPA equations are solved self-consistently so that the fundamental conservation laws are ensured. The effects related to the electron-hole symmetry in the Coulomb drag physics have been generalized to the nonlinear transport regime. A set of symmetry-induced relations linking physical quantities with the particle distribution were established on generic footing and, remarkably, they are found robust against uniformly distributed impurities. As an application, the theoretical formalism is employed to analyze the Coulomb drag transport physics in quasi-one-dimensional systems. The dependencies of the drag current on external bias, chemical potential, temperature, and the system sizes are predicted.

DOI: 10.1103/PhysRevB.99.035423

I. INTRODUCTION

Two conductive many-electron systems placed closely while kept insulated from each other can exhibit a quantum drag phenomenon due to the Coulomb interaction between the electrons [1]. Namely, a charge current passing through one of the subsystems—called the active layer (AL)—exerts a "frictional" force on the other subsystem called the passive layer (PL). If the two ends of the PL are connected to the outside world, a drag current emerges in the PL circuit (Fig. 1). This drag phenomenon has been ubiquitously observed in systems of different dimensions and geometries, including parallel metallic plates [2], quantum wells [3], wires [4,5], dots [6,7], and dimensionally hybrid systems [8,9]. The underlying physical mechanism for the Coulomb drag effect depends on the specific system dimension and the experimental setup. As suggested in early theoretical works regarding bilayer quantum wells, the drag effect was attributed to the interlayer momentum transfer due to the long-range Coulomb interaction [10,11] whereas in parallel quantum dots it was more natural to interpret the induced drag current as a rectification effect due to intrinsic fluctuations in the AL [12,13]. These two seemingly different points of view, usually referred to as the conventional drag mechanism as a whole, turn out to be closely related [1,13,14]. On the other hand, unconventional mechanisms that take into account physical processes of different origins or exotic effects in non-Fermi-liquid systems were also studied in a variety of contexts [5,15–21].

The theory of Coulomb drag physics is commonly based on the Kubo formula [10,22] and the kinetic equations [23–27]. The former is applicable in the linear response regime and the latter is most conveniently used in translational invariant or spatially continuous models. To handle the nonlinear regime far from equilibrium for nanoscale devices where the microscopic structural details can significantly influence the transport, a real-space formalism is needed that takes atomistic level parameters as input and handles an explicit voltage drop across the device. In this regard, attempts of using the quantum master equation [12,18,28] and the nonequilibrium Green's function (NEGF) theory under random phase approximation (RPA) [29] have recently been made for analyzing the drag phenomenon in small quantum dots.

It is the purpose of this paper to further develop the real-space nonequilibrium transport formalism for the Coulomb drag problem in geometries elongated along the transport direction, and to take into account the possible coexistence of random impurities in the drag system. On the one hand, disorder exists in realistic samples but its effect on the drag phenomenon has not been predicted at nonequilibrium. On the other hand, the rich physics lying in the interplay between disorder and Coulomb interaction generated persistent interests for a long time [30]. In the presence of disorder, one usually requests the averaged physical quantities over an ensemble of samples to draw general conclusions. Although modeling a disordered system under a given impurity distribution merely amounts to adjusting the single-body Hamiltonian, the disorder-averaging problem is virtually at the many-body level, which makes the theoretical problem more involved [31]. To overcome the difficulty, perturbation methods [10,14,32,33] and numerical statistics [22] were used in previous works. For practical simulations at the atomistic level, a more general and numerically efficient technique is in order for the disorder-averaging purpose.

In this paper, we deal with the electron-electron interaction using the self-consistent GW approximation [34,35]. The GW approximation, derived from RPA, is one of the classic methods for incorporating quantum effect of charge

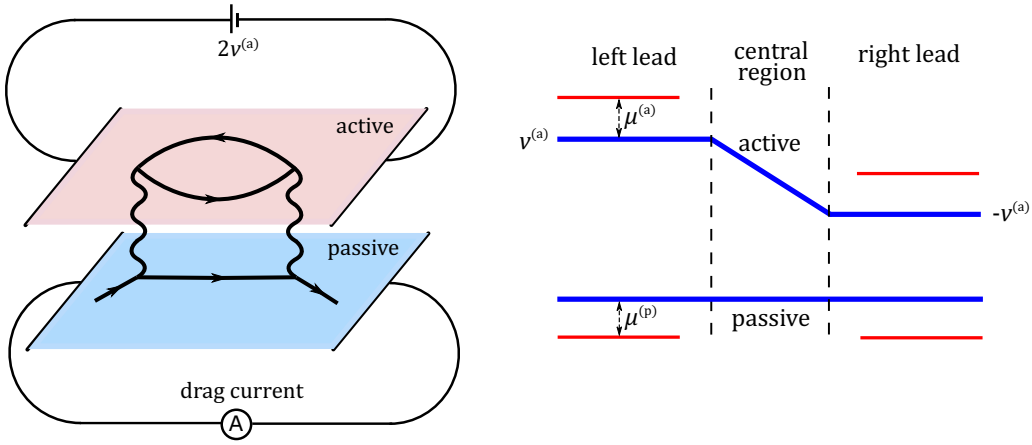

FIG. 1. Left panel: Schematic diagram of the Coulomb drag setup. A potential bias is applied across the active layer and the drag current is measured in the passive layer. The lowest order process contributing to the drag is depicted with the corresponding Feynman diagram, where solid lines with arrows denote the electron propagators and the wavy lines represent the Coulomb interaction. Right panel: Diagram of the potential profile in individual subsystems. Blue line: Electrostatic potential. Red line: Chemical potential measured with respect to certain reference points in the band structure.

fluctuations, which plays a central role in the Coulomb drag physics [1,14,36]. Another virtue of GW is that the required numerical self-consistency ensures a number of conservation laws [37–39] which typically improve the reliability of the numerical transport calculations. As for disorder-averaging, we resort to the coherent potential approximation (CPA) devised for the impurity disorder of diagonal type [40,41]. It is remarkable that CPA essentially shares the same spirit as the dynamical mean-field theory and thus goes beyond perturbative methods [31,42]. In conjunction with NEGF, GW and CPA have recently been extended into the nonequilibrium regime, respectively [43–45]. Both methods have been successfully applied to the transport simulation of a wide variety of nonequilibrium systems [45–52]. In this paper, we combine GW and CPA together so that the electron-electron interaction and disorder-average can be dealt with at the same time, and we apply this formalism to the Coulomb drag problem in disorder-containing quasi-one-dimensional transport systems.

The rest of the paper is organized as follows. The theoretical model, analysis, and the numeric simulation methods are formulated in Sec. II. The generic features of quantum drag transport are analyzed and we present a set of electron-hole symmetry relations in terms of nonequilibrium quantities. In Sec. III, we apply the formalism to a tight-binding model with different geometries. The dependence of drag currents on a number of physical parameters is studied.

II. THEORY

In what follows, the term "current" refers to the negatively charged current unless otherwise specified: its unit is e/h. To lighten the notation, we set $e = \hbar = k_B = 1$. Spin degeneracy is assumed in this paper.

A. Model Hamiltonian and general formulation

In our nonequilibrium drag model, the two-terminal configuration for quasi-one-dimensional transport is adopted for both AL and PL (Fig. 2). Each semi-infinite lead is assumed to be maintained in its thermal equilibrium while the finite central region is treated quantum mechanically [53]. The noninteracting Hamiltonian of AL (label a) and PL (label p) has the quadratic form

$$H_0^{(a/p)} = \sum_{i,j\in\text{cen}} \tau_{ij} d_i^{\dagger(a/p)} d_j^{(a/p)} + \sum_{k,l\in\mathcal{L},\mathcal{R}} \gamma_{kl} c_k^{\dagger(a/p)} c_l^{(a/p)} + \sum_{k\in\mathcal{L},\mathcal{R};i\in\text{cen}} (\beta_{ki} c_k^{\dagger(a/p)} d_i^{(a/p)} + H.c.), \quad (1)$$

respectively, where $d_i^{\dagger(a/p)}$ ($d_i^{(a/p)}$) denotes the creation (annihilation) operator for an electron on the ith site in the central region of AL/PL, $c^\dagger$ (c) creates (annihilates) an electron in the left ($\mathcal{L}$) or right ($\mathcal{R}$) leads, and the Greek letters denote the corresponding hopping matrices. Since interlayer hopping is prohibited, electrons are constrained in their respective layers. The disorder effect is considered present in the central regions of AL and PL, and it is modeled by uncorrelated random

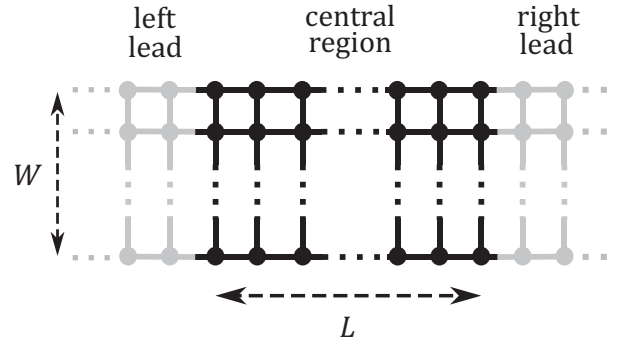

FIG. 2. Schematic drawing of a one-dimensional ribbon sliced from a square lattice. The width of the ribbon (number of rows) is denoted by W and the length of the central region is denoted by L.

variables added to the diagonal of the hopping matrix τ:

$$H_{\rm imp} = \sum_{i\in {\rm AL}} \varepsilon_i^{(a)} \hat{n}_i^{(a)} + \sum_{j\in {\rm PL}} \varepsilon_j^{(p)} \hat{n}_j^{(p)}, \tag{2}$$

where $\hat{n}_i^{(a/p)} = d_i^{\dagger(a/p)} d_i^{(a/p)}$. Finally, the interlayer interaction, assumed to be confined within the central region [22,39,53], is modeled by

$$H_{ee} = \sum_{i\in {\rm AL},\ j\in {\rm PL}} \frac{u}{|\vec{r}_i - \vec{r}_j|} \hat{n}_i^{(a)} \hat{n}_j^{(p)}, \tag{3}$$

where the parameter u scales the interaction strength. The intralayer Coulomb interaction is not explicitly considered as we assume that its effect has been absorbed into the band structure renormalization for the quasiparticles [22]. With these considerations, the total Hamiltonian of the drag system reads $H = H_0^{(a)} + H_0^{(p)} + H_{ee} + H_{\rm imp}$.

The central task of a nonequilibrium many-body problem is to calculate the retarded (R), lesser ($<$), and greater ($>$) components of NEGF, which can be obtained from the Dyson and the Keldysh equations [53]:

$$G^R(\omega) = \left[\omega I - H_0 - \Sigma^R_{\rm lead} - \Sigma^R_{\rm CPA} - \Sigma^R_{\rm GW}\right]^{-1}, \tag{4a}$$

$$G^{</>}(\omega) = G^R\left[\Sigma^{</>}_{\rm lead} + \Sigma^{</>}_{\rm CPA} + \Sigma^{</>}_{\rm GW}\right]G^{R\dagger}. \tag{4b}$$

In our notation, quantities without explicit indices are understood as matrices in the real-space basis representation of the central region. Σ denotes self-energies of different origins. The lead's self-energy $\Sigma_{\rm lead}(=\Sigma_{\mathcal{L}} + \Sigma_{\mathcal{R}})$ originates from the open boundary condition at both ends of the transport system and can be computed with the standard numerical algorithm as detailed in Ref. [54]. $\Sigma_{\rm CPA}$ and $\Sigma_{\rm GW}$, to be introduced in Secs. II B and II C, respectively, are associated with the disorder-average and the electron-electron interaction effects.

To calculate the drag effect, a voltage bias is applied across AL (Fig. 1), $v^{(a)}_{\mathcal{L}/\mathcal{R}} = \pm v^{(a)}$: They are set at opposite values, which is always doable due to the gauge invariance. The electrostatic potential in the central region (cf. right panel of Fig. 1) is assumed to be linear since electrons are subjected to frequent scattering in the presence of impurities and the Coulomb interaction [55]. On top of the bias voltage, we define another variable $\mu^{(a)}$ representing the relative position of the chemical potential with respect to the band structure of respective leads. Throughout this paperwork, the relative chemical potentials are set to be equal in both leads. For the PL, a flat potential is applied (i.e., no bias) and again $\mu^{(p)}$ is set equal in both leads. Thus, in the setup displayed in Fig. 1, one expects the Coulomb drag to induce a steady current flowing through PL in response to the nonequilibrium bias applied across AL.

B. Coherent potential approximation

In this subsection, we present our CPA approach to the disorder-average. In the Green's function theory for the disorder problem, one usually seeks an effective medium where the dressed propagator characterizes the typical behavior of a real particle encountering random scatterers in the lattice. Consider a single site in the medium denoted by i. All degrees of freedom in the rest of the lattice can be integrated out, so that the coupling between this site and the rest can be parameterized by a single variable Δ_i, expanded as $\left(\begin{smallmatrix} \Delta_i^R & \Delta_i^< \\ 0 & \Delta_i^{R*} \end{smallmatrix}\right)$ in the Keldysh space [31]. This single-site problem can be solved readily by computing the mean value of the Green's function [31,44]:

$$G_i(\omega) = \int d\varepsilon_i\, p(\varepsilon_i)[\omega I_{2\times 2} - \varepsilon_i I_{2\times 2} - \Delta_i(\omega)]^{-1}, \tag{5}$$

where ε_i is the random impurity potential and $p(\varepsilon_i)$ denotes its probability distribution. Alternatively, one can think of this site being occupied by an artificial atom with the complex potential σ_i satisfying

$$G_i(\omega) = [\omega I_{2\times 2} - \sigma_i(\omega) - \Delta_i(\omega)]^{-1}. \tag{6}$$

CPA consists of approximating the effective medium self-energy $\Sigma_{\rm CPA}$ with $\sum_i \sigma_i$, which, together with Eqs. (4), (5), and (6), forms a closed set of equations given a fixed $\Sigma_{\rm GW}$ [44].

C. GW approximation

In this section, we outline the main procedure of the nonequilibrium GW approximation for the Coulomb interaction. Details can also be found in Ref. [45]. We start with the lesser and greater polarizations,

$$P^{</>}_{ij}(\omega) = -2i \int \frac{d\omega'}{2\pi} G^{</>}_{ij}(\omega+\omega') G^{>/<}_{ji}(\omega'), \tag{7}$$

which serve as an intermediate quantity for the GW calculation. The retarded polarization is obtained from the Kramers-Kronig relation [56]:

$$P^R_{ij}(\omega) = i \int \frac{d\omega'}{2\pi} \frac{P^>_{ij}(\omega') - P^<_{ij}(\omega')}{\omega - \omega' + i0^+}. \tag{8}$$

Note that in our problem, as particle interchange is prohibited between AL and PL, the real-space indices attached to the polarization or the Green's functions must lie in the same layer. Next, the screened interaction is computed as

$$W^R(\omega) = [I - V P^R(\omega)]^{-1} V, \tag{9a}$$

$$W^{</>}(\omega) = W^R(\omega) P^{</>}(\omega) W^R(\omega)^\dagger. \tag{9b}$$

Exploiting the bipartition nature of the drag system, these quantities can be viewed as in the two-by-two matrix form:

$$W = \begin{pmatrix} W^{aa} & W^{ap} \\ W^{pa} & W^{pp} \end{pmatrix},\ P = \begin{pmatrix} P^a & 0 \\ 0 & P^p \end{pmatrix},\ V = \begin{pmatrix} 0 & U \\ U^\dagger & 0 \end{pmatrix},$$

where $U_{ij} = u/|\vec{r}_i - \vec{r}_j|$ [see Eq. (3)], and hence the matrix operations in Eq. (9) can be resolved with smaller matrices. The GW method consists of approximating the interaction self-energy as

$$\Sigma^{</>}_{{\rm GW},ij}(\omega) = i \int \frac{d\omega'}{2\pi} G^{</>}_{ij}(\omega-\omega') W^{</>}_{ij}(\omega'). \tag{10}$$

The retarded self-energy is again derived from the Kramers-Kronig relation Eq. (8), with P replaced by $\Sigma_{\rm GW}$. Finally, the self-energy is inserted into the Dyson and the Keldysh Eqs. (4) to obtain the Green's functions. This closes the loop of one GW iteration.

In terms of numerical implementation, all the quantities are stored as matrices aligned on an energy grid with equal spacing. The convolution integrals in Eqs. (7), (8), and (10) are computed with the fast Fourier transform (FFT) [45,57], and a parallelization over the real-space indices is implemented. The computations of Eqs. (4) and (9), as well as the CPA calculation, are parallelized over the energy points. In practice, to arrive at the simultaneous convergence of the GW and the CPA calculations, our numerical program proceeds as follows. It starts with an initial guess for the GW self-energy and solves the CPA equations iteratively until convergence. The outcome Green's function is then used to carry out the GW calculation. Next, the GW self-energy is updated with a Pulay mixer [58,59] followed by a repeated CPA calculation since the underlying Σ_{GW} has been changed. The entire procedure is iterated until an overall convergence (in both CPA and GW self-energies) is achieved.

D. Drag current

Having established the combined formalism of CPA and GW for the drag system, one can easily understand the central question of how the PL "crosstalks" with the AL and hence "knows" about its nonequilibrium status. The GW theory provides a concrete physical picture to answer this question. First, the nonequilibrium statistical information in the AL is encoded in its charge fluctuation, represented by the polarization [Eq. (7)]. Then, through the dynamical screening process [53] the fluctuation reshapes the Coulomb interaction [Eq. (9)] so that the interlayer medium carries the information about AL. PL receives this information from the medium via the process described by Eqs. (4) and (10), and hence makes response to the driving "force."

In the NEGF formalism, the current through lead $\alpha(=\mathcal{L}$ or $\mathcal{R})$ of either subsystem can be calculated as

$$I_\alpha^{(a/p)} = \int d\omega J_\alpha^{(a/p)}(\omega),$$

where the energy resolved current density $J_\alpha^{(a/p)}(\omega)$ is defined as [53]

$$J_\alpha^{(a/p)}(\omega) = \mathrm{Tr}\left(G^{>(a/p)}\Sigma_\alpha^{<(a/p)} - G^{<(a/p)}\Sigma_\alpha^{>(a/p)}\right).$$

The first and the second terms on the right-hand side represent the electron and the hole current, respectively. The three typical profiles of $J_{\mathcal{L}}^{(p)}(\omega)$ are sketched in Fig. 3. In our calculations, we find that the electron drag current is always accompanied by a codirectional hole current of about the same magnitude, and vice versa. Therefore, the measurable drag current merely arises from the slight difference between the two currents. This manifests the different origin of the Coulomb drag current compared to the regular field driven current.

As both GW and CPA have proven to be Φ-derivable approximations, charge conservation is ensured as long as the GW and CPA equations are solved self-consistently [31,39]. As a result, we have the identity $I_{\mathcal{L}}^{(a/p)} + I_{\mathcal{R}}^{(a/p)} = 0$, which has been checked throughout our calculations to provide a very strict verification of the numerical procedure.

It should be pointed out that the formalism presented here only takes into account the delocalized electronic states in the transport system [45]. Note that, since charge fluctuation involves all the quantum states within the relevant energy window, the localized states lying in there should also participate in the drag process [60]. In this paper, we consider disorder scattering effects away from any localization regime.

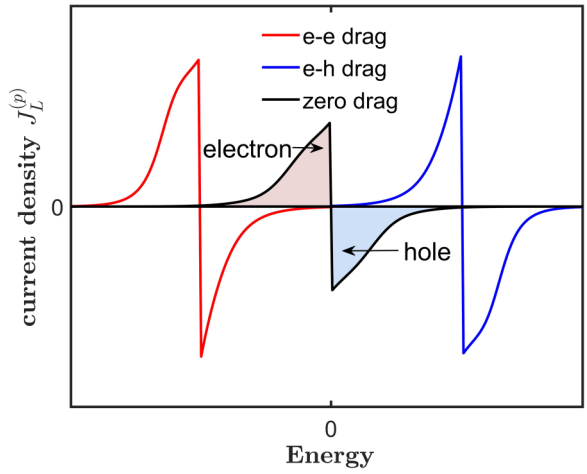

FIG. 3. Typical profiles of the energy-resolved current density in the left lead of the passive layer ($J_{\mathcal{L}}^{(p)}(\omega)$). Black curve: $J_{\mathcal{L}}^{(p)}(\omega)$ at the electron-hole symmetric point where the hole current (shaded area below the zero axis) cancels out the electron current (shaded area above the zero axis). Red curve: $J_{\mathcal{L}}^{(p)}(\omega)$ of electron-electron (e-e) drag where the electron current exceeds the hole current, yielding a positive total current. Blue curve: $J_{\mathcal{L}}^{(p)}(\omega)$ of electron-hole (e-h) drag, which yields a negative total current. $J_{\mathcal{L}}^{(p)}(\omega)$ switches its sign at $\omega = \mu^{(p)}$.

E. Electron-hole symmetry

Within the linear response or the kinetic equation approach, it has been theoretically confirmed that the direction of the drag current can be influenced by varying the relative occupation of electrons and holes in the system and that, particularly, according to the conventional Coulomb drag theory, the drag current vanishes when the chemical potential is set right at the electron-hole symmetric point [1,14,23,61]. In this paper, such phenomena have been generalized for the nonequilibrium drag where analyses from previous works, solely based on the band structure symmetry, cease to be valid. This emergent *nonequilibrium* electron-hole symmetry has been confirmed in our numerical simulation.

The central result of this subsection is that the drag current is an odd function with respect to either $\mu^{(a)}$ or $\mu^{(p)}$:

$$\begin{aligned} I_{\mathcal{L}}^{(p)}(\mu^{(a)}, \mu^{(p)}) &= -I_{\mathcal{L}}^{(p)}(-\mu^{(a)}, \mu^{(p)}) \\ &= -I_{\mathcal{L}}^{(p)}(\mu^{(a)}, -\mu^{(p)}) = I_{\mathcal{L}}^{(p)}(-\mu^{(a)}, -\mu^{(p)}), \end{aligned} \tag{11}$$

given the sufficient condition that (i) the atomic structure and the hopping Hamiltonian of both AL and PL subsystems bear inversion symmetry about the center of the device, (ii) the electrostatic potential in AL is odd about the center of the device while that in PL is zero everywhere, and (iii) the leads of respective subsystems are identical and have a symmetric band structure. Remarkably, Eq. (11) remains true even for

the disorder averaged current, providing that the probability distribution of the impurity potential is even: $p(\varepsilon_i) = p(-\varepsilon_i)$. The detailed derivation for Eq. (11) is presented in the Appendix.

III. NUMERICAL RESULTS

In this section, we present numerical results for the tight-binding model of Fig. 2. The structures of AL and PL are chosen to be identical. The interlayer distance is set to be equal to the site spacing a. Hopping is allowed only between nearest neighbors with an identical amplitude t. The resulting band structure is plotted in Fig. 11 of Appendix B for reference. This model can be interpreted as a real-space finite-difference representation for the effective Hamiltonian of semiconductor wires [22,55]. To be specific, the hopping amplitude is estimated from $t = \hbar^2/2m^*a^2$, where m^* is the effective mass, and the interaction strength $u = e^2/4\pi\epsilon_0\epsilon_r a$. As a concrete example to illustrate the parametrization of our model, when a grid spacing of 2.5nm is used the u parameter for a GaAs wire would become $u = 0.5t$ [62]. To lighten the notation, t is taken as the energy unit henceforth, and the half-filling point of the band structure is chosen as the reference point. To simulate the disorder effect, we allow the on-site energy of each atom to take either of the two values, ε or $-\varepsilon$, with an identical probability. The temperature parameter is set at $k_BT = 0.001$ in all leads, unless otherwise specified. In addition, the relative chemical potentials in all leads are set equal: $\mu^{(a)} = \mu^{(p)}$. The numerical accuracy of our formalism is essentially controlled by the range and the spacing of the energy grid used in the GW calculation. For the numerical results presented in this section, a proper grid ranging from -18.0 to 18.0 with a spacing no larger than 0.01 is tested to be adequate. In addition, extra zero-padding is added when the FFT facilitated convolutions are carried out [45,57].

A. Drag current versus bias and chemical potential

We first present results for the simplest chain model ($W = 1$) with four interacting sites in the central region ($L = 4$). The interaction and disorder strengths are set at $u = 2.0$ and $\varepsilon = 0.2$, respectively. We sweep the AL bias $v^{(a)}$ from 0.0 to 1.0, and the chemical potential $\mu^{(a/p)}$ from 0.0 to 1.8. At each pair of $v^{(a)}$ and $\mu^{(a/p)}$, a self-consistent calculation is performed and the computed drag current $I^{(p)}$ (in units of e/h) is recorded. The numerical results are presented in Fig. 4.

Regarding the bias dependence of the drag current at a fixed $\mu^{(a/p)}$, the negative differential conductance previously reported in Ref. [29] is not found in our model. The system studied in Ref. [29] consists of quantum dots weakly coupled to the leads, so that the transport property is rather sensitive to the position of individual energy levels in the dot. In contrast, our drag model closely mimics the transport in quantum wires rather than dots. The dependence of $I^{(p)}$ on $\mu^{(a/p)}$ at a few selected $v^{(a)}$'s is shown in the right panel of Fig. 4. The drag current starts at zero, as required by the electron-hole symmetry at $\mu^{(a/p)} = 0$, increases monotonously and then decreases as $\mu^{(a/p)}$ approaches the vicinity of the band edge. Numerically, it is unclear whether the drag current will continue decreasing all the way up to the band edge, since

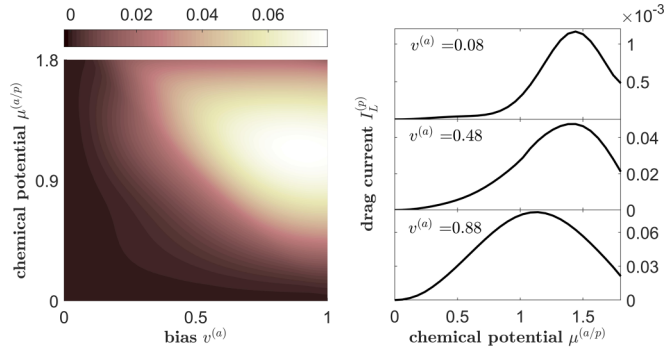

FIG. 4. Drag current in the chain model ($L = 4$) versus the bias voltage $v^{(a)}$ and chemical potential $\mu^{(a/p)}$. The interaction and the disorder strengths are set at $u = 2.0$ and $\varepsilon = 0.2$, respectively. Left panel: 2D plot of the drag current $I^{(p)}$ versus $v^{(a)}$ and $\mu^{(a/p)}$. Right panel: Cuts at a few selected $v^{(a)}$.

some earlier theoretical works [26,27] suggested that the drag current should sharply peak at the band edge. We found that our self-consistent GW calculation became very hard and even failed to converge at certain points when $\mu^{(a/p)}$ is extremely close to the band edge, which is plausibly caused by such sharp discontinuity.

Next, we move on to the study of a ribbon structure with $W = L = 4$. The range of $\mu^{(a/p)}$ is increased up to 3.0 for adaption to the change in the band structure. Other parameters remain the same as in the chain model. The results are shown in Fig. 5. As can be seen, the dependence of drag currents on $v^{(a)}$ and $\mu^{(a/p)}$ becomes much more complicated than that for the chain model. This mainly results from the underlying multiband structure of the ribbon. An associated observation is that, as shown in the right panel of Fig. 5, at a low bias (e.g., $v^{(a)} = 0.08$) the drag current peaks close to the subband edges of the noninteracting Hamiltonian (marked by dashed lines). This interesting finding qualitatively agrees with the results from the kinetic theory [26,27]. The noticeable broadening of these peaks and their deviation from the exact positions can be attributed to the many-body renormalization of the electronic structure. On the other hand, in the far-from-equilibrium

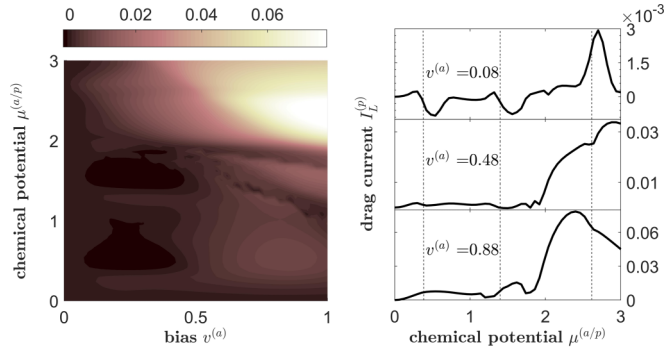

FIG. 5. Drag current in the ribbon model ($W = L = 4$) versus the bias voltage $v^{(a)}$ and chemical potential $\mu^{(a/p)}$. The interaction and the disorder strengths are set at $u = 2.0$ and $\varepsilon = 0.2$, respectively. Left panel: 2D plot of the drag current $I^{(p)}$ versus $v^{(a)}$ and $\mu^{(a/p)}$. Right panel: Cuts at a few selected $v^{(a)}$. Subband edges of the noninteracting Hamiltonian are marked by dashed lines.

regime (e.g., $v^{(a)} = 0.48, 0.88$) which has not been studied before, these peaks cease to be distinguishable.

All the computations have been repeated for the same structures under the condition $\varepsilon = 0$, and no qualitative difference has been found.

B. Drag current versus the length of the central region

It is well-known that Coulomb interaction and impurity disorder conspire to complicate as well as enrich the Coulomb drag physics [1]. On the one hand, the drag effect due to Coulomb interaction should grow as the scattering region enlarges [22]. On the other hand, impurity scattering hinders electronic transport in general. Therefore, it is interesting and necessary to investigate the dependence of drag currents on the system length so as to explore the interplay between the Coulomb interaction and the disorder effect.

We first present in Fig. 6 (left column) the numerical results for the drag current ($I^{(p)}$) calculated under a relatively small bias ($v^{(a)} = 0.05$). For each system (distinguished by its width W), the chemical potential and the Coulomb interaction strength are fixed at a certain value, respectively (see the caption of Fig. 6) whereas the length of the scattering region and the impurity energy are varied. It has been shown with the kinetic approach that, in the ballistic limit, the drag transconductance should grow monotonously with increasing length (L) in the asymptotic regime [26]. As can be seen, our result for the disorder-free ($\varepsilon = 0.0$) samples qualitatively agrees. Furthermore, our numerical calculation suggests that, even in the presence of impurities, the $I^{(p)} - L$ relation could remain increasing up to a rather large L.

To investigate the $I^{(p)} - L$ relation in the far-from-equilibrium regime, we have computed the drag currents under a relatively large bias ($v^{(a)} = 0.5$). The numerical results are shown in the right column of Fig. 6. Interestingly, we find that impurity scattering gets more pronounced in this regime than in the low bias case: in the weak disorder regime ($\varepsilon < 0.2$), the far-from-equilibrium drag current again grows with increasing length, whereas in the presence of stronger disorder the drag current tends to decrease after a certain length [see Figs. 6(b) and 6(d), particularly]. Furthermore, such disorder-induced impediment is found related to the width of the system: in the chain model with $\varepsilon = 0.5$, the point where the drag current starts to decrease is at $L = 20$ [Fig. 6(b)], whereas in the ribbon with $W = 2$ the turning point shifts to a larger value $L = 30$ [Fig. 6(d)]. Such observation is consistent with the classical size dependence of the disorder-induced resistance.

Along with the drag currents, the drive currents in AL have also been calculated in our simulations. Their typical behavior is illustrated in Fig. 7, where the numerical result for the chain model under $v^{(a)} = 0.5$ is displayed [from the same calculation as for Fig. 6(b)]. The drive current can be hindered by both Coulomb and impurity scattering processes. The effect of the former is well manifested in the disorder-free limit (the dark blue curve in Fig. 7). In this limit, the drive current is found to decrease with increasing length in the monotonous increasing region of the drag current, which is consistent with the interlayer momentum transfer picture. In the presence of disorder, both scattering processes contribute so that the drive current decreases monotonously with increasing length.

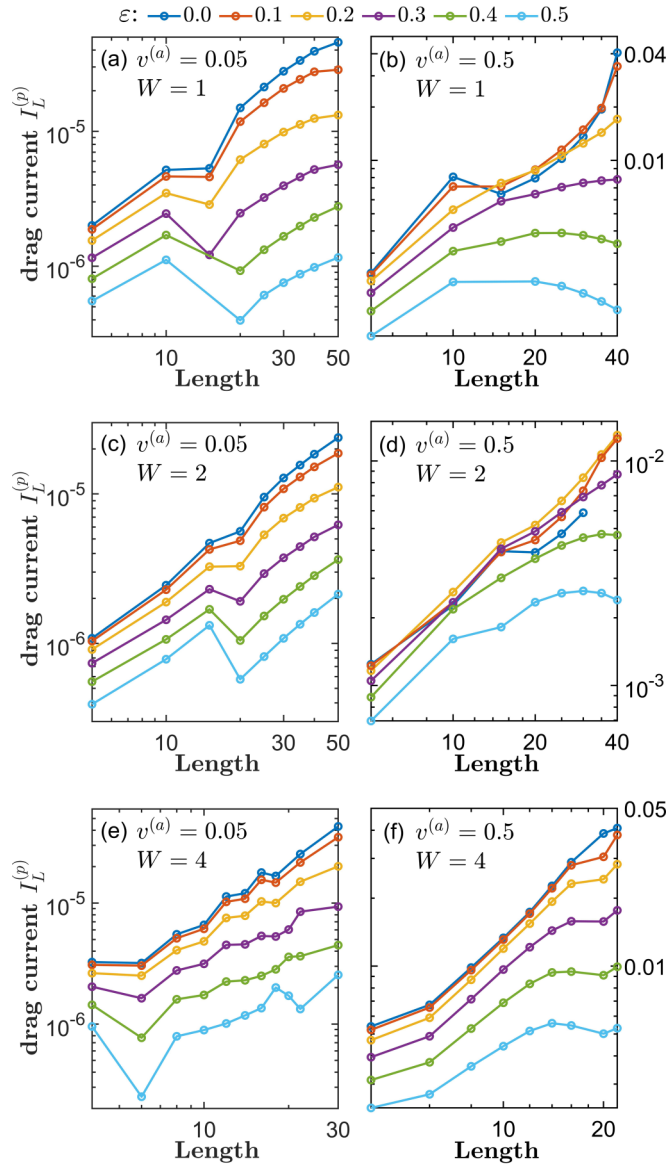

FIG. 6. Drag currents versus the length of the central region in systems of different widths. The chemical potentials are set at $\mu^{(a/p)} = 1.0, 2.0, 2.0$ for $W = 1, 2, 4$, respectively. Both low ($v^{(a)} = 0.05$) and high ($v^{(a)} = 0.5$) bias voltages are applied. The interaction is set at $u = 0.5$ and the impurity energy ε is varied from 0.0 to 0.5, labeled with different colors.

C. Drag current versus temperature

It has been shown theoretically that the generic feature of quantum drag transport is highly associated with temperature. When the temperature is significantly higher than the voltage bias (the linear regime), the drag effect mainly arises from the rectification of nearly equilibrium thermal fluctuations and thus it should grow with increasing temperature [1]. In the opposite limit (the nonlinear regime), the drag transport is determined solely by the intrinsic electronic structure of the device [1].

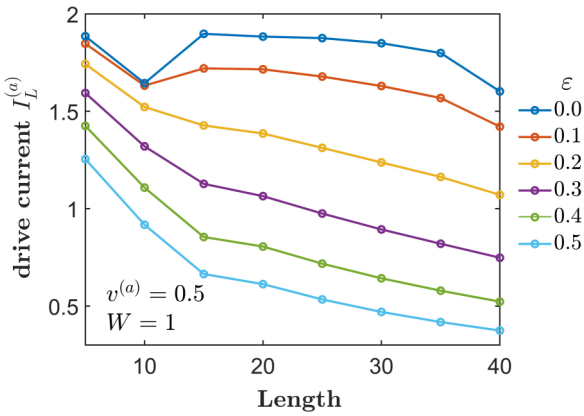

FIG. 7. Drive current versus the length of the central region of the tight-binding chain model. The impurity energy ε is varied from 0.0 to 0.5, labeled with different colors. Other parameters: $v^{(a)} = 0.5$, $u = 0.5$, $\mu^{(a/p)} = 1.0$.

In this subsection, by applying a low bias ($v^{(a)} = 0.01$) on AL and varying the temperature from low to high, we investigate the temperature dependence of the drag transport in both regimes plus the crossover in between. Systems of two different geometries are considered: A chain with $L = 25$ and a ribbon with $W = 4$, $L = 10$. The relative chemical potential is set at $\mu^{(a/p)} = 1.0$ in the chain model and $\mu^{(a/p)} = 2.0$ in the ribbon. The disorder strength is varied from $\varepsilon = 0.0$ to 0.5 while the interaction strength is fixed at $u = 1.0$ in both systems. The results are presented in Fig. 8. At intermediate temperatures ($v^{(a)} < k_BT \ll \mu^{(a/p)}$), for both systems we observe a power law increase of the drag current versus the temperature, which suggests that the drag transport is more of a thermal rectification effect [1]. The rapidness of such increase is found dependent on the disorder strength, as clearly shown in Fig. 8(a). As the temperature decreases, the system is then driven toward the nonlinear regime where the thermal rectification ceases to play a major role [1]. As can be seen, in the regime $k_BT \ll v^{(a)}$ the drag current tends to

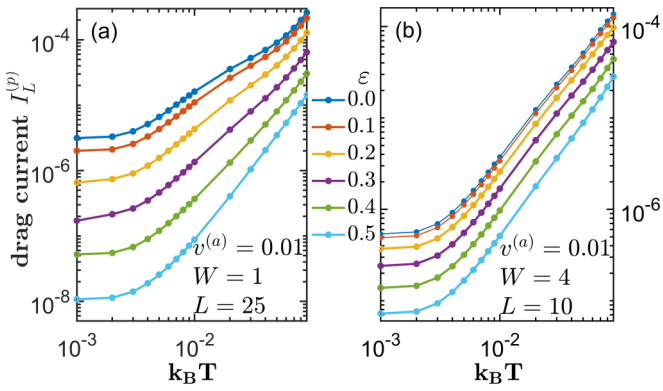

FIG. 8. The temperature dependence of the drag current under $v^{(a)} = 0.01$ in a chain model with $L = 25$ (left panel) and a ribbon with $W = 4$, $L = 10$ (right panel). The relative chemical potential is set at $\mu^{(a/p)} = 1.0$ in the chain model and $\mu^{(a/p)} = 2.0$ in the ribbon. The interaction strength is set at $u = 1.0$ while the disorder strength is varied from $\varepsilon = 0.0$ to 0.5.

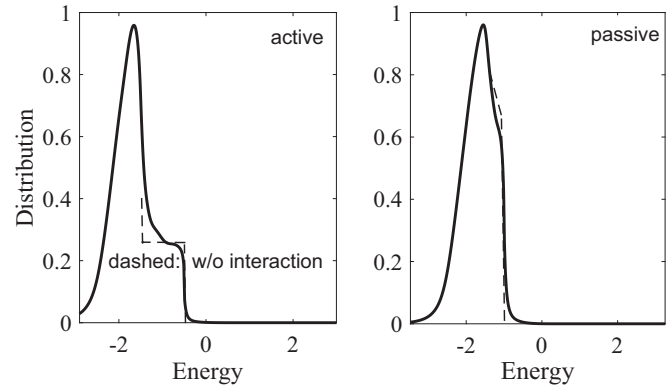

FIG. 9. Respective energy distribution (particle occupation) at the center of a pair of disorder-free chains of length $L = 20a$. The active subsystem is driven out of equilibrium under $v^{(a)} = 0.5$. Other parameters: $u = 0.5$, $\mu^{(a/p)} = -1.0$.

saturate at a nonzero value, which indicates that the nonlinear drag transport can exist even without thermal fluctuations [1].

D. Further discussions

An important aspect of the Coulomb drag physics is the nonequilibrium distribution of electrons in the two wires. The nonequilibrium distribution in the AL delivers a "driving force" for a steady-state drag current to flow in the PL. This distribution has a tendency of equilibration due to inelastic scattering which transfers energy between the two subsystems. To this end, a self-consistent calculation of the distribution is necessary [63] and in the NEGF formalism presented above, it is done by self-consistently solving the coupled Dyson-Keldysh equation [cf. Eq. (4)] for $G^<$ under proper transport boundary conditions [53]. Figure 9 shows the calculated particle occupation (the diagonal of $\mathrm{Im}G^<$) at the center of a pair of disorder-free chains. The smearing of

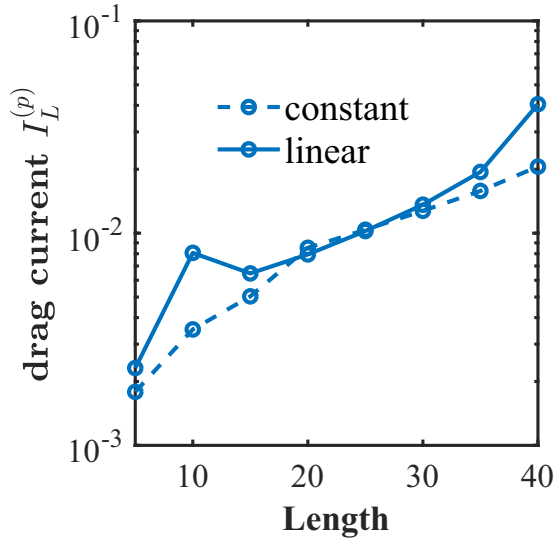

FIG. 10. Drag currents versus the length, computed under differing electrostatic potential profiles (i.e., constant versus linear). Model parameters are same as in Fig. 6(b).

the self-consistent distribution against sharp-steps (dashed) signifies the energy relaxation effect which tends to equilibrate the active chain while driving the passive chain out of equilibrium.

So far, in the numerics we assumed a linear electrostatic potential profile along the AL due to the external bias voltage. To what extent could this profile affect the computed results? To this end, we recalculate for the case of the dark blue curve of Fig. 6(b), but this time with an electrostatic potential along AL set to be a constant instead of linear. The comparison is shown in Fig. 10 and the overall agreement of the two results is qualitatively very good and semiquantitatively reasonable. Nevertheless, we argue that the linear potential profile is qualitatively better for describing realistic situations because the inevitable inelastic scattering tends to drive the profile away from a constant shape. Ultimately, a quantitative solution of the electrostatic potential profile can be obtained by solving the Poisson equation [64].

IV. SUMMARY

We have presented a theoretical formalism for analyzing the quasi-one-dimensional Coulomb drag problem in general two-terminal transport systems. The input of our theory consists of experimentally controllable variables only and no phenomenological parameters such as relaxation time or mean free path are needed for describing the elementary scattering processes.

The dependence of the drag effect on a number of variables has been investigated. For the temperature dependence, we find that the linear drag current at $k_BT > v^{(a)}$ exhibits a power law decrease with decreasing temperature. At $k_BT \sim v^{(a)}$ the drag effect crosses over toward the nonlinear regime as the temperature decreases. At $k_BT \ll v^{(a)}$ the drag current saturates at a nonzero value. For the chemical potential dependence, the drag current under low bias is found sensitive to its position with respect to subband edges, whereas this behavior fades out as the drive voltage increases.

Our real space formalism allows us to investigate the important problem of how the drag current varies with the length of the disordered scattering region. Our numerical results for drag currents under low bias qualitatively agree with the theoretical prediction previously derived in the ballistic limit [22,26]: The drag current increases with increasing length. Our calculation suggests that such increasing trend could persist even in the presence of disorder, as long as the drive bias is relatively low. In contrast, in the far-from-equilibrium regime, as the length increases the drag current exhibits a downturn due to the impurity scattering and the turning point is dependent on the system width.

The electron-hole symmetry/asymmetry is known to play an important role in the Coulomb drag physics. On this aspect, first we have demonstrated that the NEGF formalism allows for computing the electron and the hole drag currents individually. Based on our numerical results, we argued that the cancellation between electron and hole drag currents constitutes a major reason for the smallness of the net drag current and that the individual contribution from either species is significantly larger in magnitude. Therefore, the key to increasing the drag current consists of enlarging the electron-hole asymmetry, for example, by using electrodes with distinct electronic properties. This insight should be useful for Coulomb drag engineering. In addition, we have derived a set of parity relations which associate the general nonequilibrium drag current with the chemical potential. We find that, provided that the underlying noninteracting Hamiltonian bears electron-hole symmetry and that the real-space structure bears inversion symmetry, inverting either chemical potential in AL or PL results in reversing the drag current.

Although the purpose of the formalism presented here is to capture the main physical processes of nonequilibrium Coulomb drag in the presence of disorder and it was applied at relatively low temperatures in this work, it should also be noted that, two additional effects would arise as temperature goes higher, namely the plasmon enhancement and the phonon mediation, which manifest on temperature scales associated with the Fermi and Debye energies, respectively [1]. An explicit treatment of *intra*layer electron-electron [65] and electron-phonon interactions [66] would be required to take into account these physical processes, for which we wish to be able to report in a future opportunity.

ACKNOWLEDGMENTS

C.Z. wishes to thank Dr. Ying-Chih Chen for useful discussions on the GW method. We gratefully acknowledge financial support by Natural Sciences and Engineering Research Council of Canada (H.G.). We thank CalcuQuebec and Compute Canada for computation facilities.

APPENDIX A: DERIVATION OF THE ELECTRON-HOLE SYMMETRY RELATIONS

In this Appendix, we elucidate the symmetry relation Eq. (11) on a generic basis.

The noninteracting Hamiltonian of a two-terminal transport model has the following block-tridiagonal form:

$$\mathbf{H}_0 = \begin{bmatrix} \ddots & \mathbf{H}_{-m-1,-m} & & & \\ \mathbf{H}_{-m,-m-1} & \mathbf{H}_{-m,-m} + \mathbf{V}_{-m} & \mathbf{H}_{-m,-m+1} & & \\ & \mathbf{H}_{-m+1,-m} & \ddots & \mathbf{H}_{m-1,m} & \\ & & \mathbf{H}_{m,m-1} & \mathbf{H}_{m,m} + \mathbf{V}_m & \mathbf{H}_{m,m+1} \\ & & & \mathbf{H}_{m+1,m} & \ddots \end{bmatrix},$$

where m labels the principle layers, $\mathbf{H}$ denotes the corresponding hopping matrices, and $\mathbf{V}$ represents the diagonal potential matrices. In AL, we have imposed $\mathbf{V}_{-m} = -\mathbf{V}_m$ while in PL we have $\mathbf{V} = 0$. For a real-space model with structural inversion symmetry, we have $\mathbf{H}_{mn} = \mathbf{H}_{-m,-n}$. In this case, eigenvectors of $\mathbf{H}_0$ emerge in pairs with opposite eigenvalues: Providing $\mathbf{\Psi}^{(\kappa)}$ is a certain eigenvector satisfying $\mathbf{H}_0\mathbf{\Psi}^{(\kappa)} = \epsilon^{(\kappa)}\mathbf{\Psi}^{(\kappa)}$, one can derive its pairing eigenvector $\mathbf{\Psi}^{(-\kappa)}$ which satisfies $\mathbf{H}_0\mathbf{\Psi}^{(-\kappa)} = \epsilon^{(-\kappa)}\mathbf{\Psi}^{(-\kappa)}$, where $\epsilon^{(-\kappa)} = -\epsilon^{(\kappa)}$ and $\psi_{-i}^{(-\kappa)*} = \psi_i^{(\kappa)}\eta_i$, i being a real-space index and η being a vector whose explicit form, although mathematically derivable, does not need to be known. Since $\mathbf{H}_0$ is real and because of the inversion symmetry, we have $|\psi_{-i}^{(-\kappa)}| = |\psi_i^{(\kappa)}|$ and thus the value of η_i can only be -1 or 1. Such eigenvector pairing reflects the physical picture that, if $\mathbf{\Psi}^{(\kappa)}$ corresponds to an electron scattering state [64] incident from one side of the device, on the other half of the spectrum there should equally exist a hole state, denoted by $\mathbf{\Psi}^{(-\kappa)}$, incident from the other side.

With the Lehmann representation, the retarded noninteracting Green's function can be formally written as [55]

$$G^R_{0,ij}(E) = \sum_\kappa \frac{\psi_i^{(\kappa)}\psi_j^{(\kappa)*}}{E - \epsilon^{(\kappa)} + i0^+}.$$

Using the symmetry of the wave function, we further get

$$G^R_{0,ij}(E) = -\eta_i\eta_j\left[\sum_\kappa \frac{\psi_{-i}^{(-\kappa)}\psi_{-j}^{(-\kappa)*}}{-E - \epsilon^{(-\kappa)} + i0^+}\right]^*.$$

The quantity in the bracket is easily recognized as $G^R_{0,-i,-j}(-E)$. Thus we find $G^R_{0,ij}(E) = -\eta_i\eta_j[G^R_{0,-i,-j}(-E)]^*$. Similarly, taking into account the respective Fermi-Dirac distributions in the leads, the lesser Green's function can be written as [67]

$$G^<_{0,ij}(\mu, E) = i\sum_{\alpha=\mathcal{L},\mathcal{R}} n_F(E-\mu_\alpha)\sum_{\kappa\in\alpha}\delta(E-\epsilon^{(\kappa)})\psi_i^{(\kappa)}\psi_j^{(\kappa)*}.$$

With some straightforward algebra, we can continue writing

$$\begin{aligned} G^<_{0,ij}(\mu, E) &= \eta_i\eta_j\sum_\alpha i[1 - n_F(-E+\mu_\alpha)] \\ &\quad\times\sum_{\kappa\in\alpha}\delta(-E-\epsilon^{(-\kappa)})\psi_{-i}^{(-\kappa)*}\psi_{-j}^{(-\kappa)} \\ &= \eta_i\eta_j[G^>_{0,-i,-j}(-\mu, -E)]^*, \end{aligned}$$

where we have used the identities $\delta(x) = \delta(-x)$ and $1/(e^x + 1) = 1 - 1/(e^{-x} + 1)$. In the particular case $\mathbf{V} = 0$, in addition to the electron-hole symmetry, there emerges another pair of scattering states incident from opposite directions with the same energy and flipped wave functions. This leads to the relations $G^R_{0,ij}(E) = G^R_{0,-i,-j}(E)$ and $G^{</>}_{0,ij}(E) = G^{</>}_{0,-i,-j}(E)$.

Putting everything into context, upon flipping the sign of the chemical potential in AL ($\mu^{(a)} \to -\mu^{(a)}$) while keeping $\mu^{(p)}$ fixed, we have the noninteracting Green's functions changed in the following way:

$$G^{R(p)}_{ij}(\mu^{(a)}, E) = G^{R(p)}_{-i,-j}(-\mu^{(a)}, E), \tag{A1a}$$

$$G^{</>(p)}_{ij}(\mu^{(a)}, E) = G^{</>(p)}_{-i,-j}(-\mu^{(a)}, E), \tag{A1b}$$

$$G^{R(a)}_{ij}(\mu^{(a)}, E) = -\eta_i\eta_j\left[G^{R(a)}_{-i,-j}(-\mu^{(a)}, -E)\right]^*, \tag{A1c}$$

$$G^{<(a)}_{ij}(\mu^{(a)}, E) = \eta_i\eta_j\left[G^{>(a)}_{-i,-j}(-\mu^{(a)}, -E)\right]^*, \tag{A1d}$$

where we have omitted the 0 subscript as later on we will see that the interacting Green's functions also follow these relations. The argument $\mu^{(p)}$ has also been omitted for simpler notations. Plugging Eqs. (A1b) and (A1d) into Eq. (7) and making use of the fact $\eta_i^2 = 1$, we get

$$\begin{aligned} P^{<(p/a)}_{ij}(\mu^{(a)}, E) &= P^{<(p/a)}_{-i,-j}(-\mu^{(a)}, E) \\ &= \left[-P^{>(p/a)}_{-i,-j}(-\mu^{(a)}, -E)\right]^*. \end{aligned} \tag{A2}$$

Applying Eq. (A2) to the Kramers-Kronig relation Eq. (8), we find

$$P^{R(p/a)}_{ij}(\mu^{(a)}, E) = P^{R(p/a)}_{-i,-j}(-\mu^{(a)}, E). \tag{A3}$$

Next, we move on to the screened interaction. From the recursive equivalent to Eq. (9a), we get

$$\begin{aligned} W^{R(aa)}(\mu^{(a)}, E) &= U P^{R(p)} U^\dagger \\ &\quad + U P^{R(p)} U^\dagger P^{R(a)} U P^{R(p)} U^\dagger + \cdots \end{aligned}$$

Taking the first term as an example, we observe

$$\begin{aligned} U P^{R(p)} U^\dagger &= U_{ik} P^{R(p)}_{kl}(\mu^{(a)}, E) U^\dagger_{lj} \\ &= U_{-i,-k} P^{R(p)}_{-k,-l}(-\mu^{(a)}, E) U^\dagger_{-l,-j}, \end{aligned}$$

where we have utilized Eq. (A3) and the trivial fact $U_{-i,-k} = U_{ik}$ due to the structural symmetry of the system. Repeated indices in the above equation should be summed over. Carrying on the same analysis for all subsequent terms, we arrive at

$$W^{R(aa)}_{ij}(\mu^{(a)}, E) = W^{R(aa)}_{-i,-j}(-\mu^{(a)}, E).$$

With some straightforward algebra, one can verify that $W^{R(ap)}$, $W^{R(pa)}$, and $W^{R(pp)}$ all follow the same relation. Using the relations

$$W^{<(aa)} = W^{R(aa)} P^{<(a)} W^{R(aa)\dagger} + W^{R(ap)} P^{<(p)} W^{R(ap)\dagger},$$

$$W^{<(pp)} = W^{R(pp)} P^{<(p)} W^{R(pp)\dagger} + W^{R(pa)} P^{<(a)} W^{R(pa)\dagger},$$

derived from Eq. (9b) together with Eq. (A2), we find that $W^{<,>}$ follows the same relation as Eq. (A2):

$$\begin{aligned} W^{<(p/a)}_{ij}(\mu^{(a)}, E) &= W^{<(p/a)}_{-i,-j}(-\mu^{(a)}, E) \\ &= \left[-W^{>(p/a)}_{-i,-j}(-\mu^{(a)}, -E)\right]^*. \end{aligned} \tag{A4}$$

Putting Eqs. (A1b), (A1d), (A4), and (10) together, we find

$$\begin{aligned} \Sigma^{</>(p)}_{\mathrm{GW},ij}(\mu^{(a)}, E) &= \Sigma^{</>(p)}_{\mathrm{GW},-i,-j}(-\mu^{(a)}, E), \\ \Sigma^{<(a)}_{\mathrm{GW},ij}(\mu^{(a)}, E) &= \eta_i\eta_j\left[\Sigma^{>(a)}_{\mathrm{GW},-i,-j}(-\mu^{(a)}, -E)\right]^*, \end{aligned} \tag{A5}$$

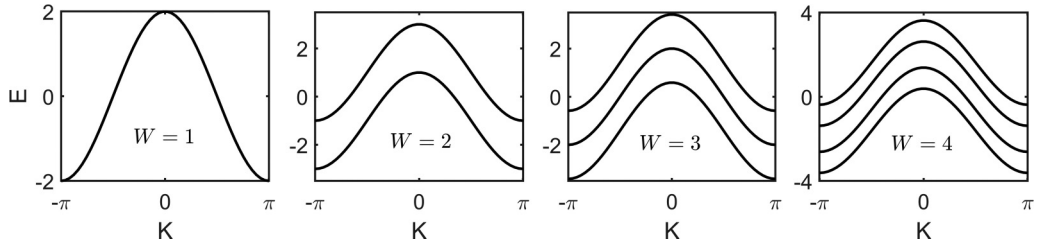

FIG. 11. Band structures of the square lattice tight-binding model described in Fig. 2 with selected widths W. The nearest-neighbor hopping amplitude is taken as the energy unit.

Using the Kramers-Kronig relation Eq. (8) again, we get

$$\Sigma^{R(p)}_{\mathrm{GW},ij}(\mu^{(a)},E)=\Sigma^{R(p)}_{\mathrm{GW},-i,-j}(-\mu^{(a)},E)$$
$$\Sigma^{R(a)}_{\mathrm{GW},ij}(\mu^{(a)},E)=-\eta_i\eta_j\big[\Sigma^{R(a)}_{\mathrm{GW},-i,-j}(-\mu^{(a)},-E)\big]^* \quad \text{(A6)}$$

Applying the relations Eqs. (A1), (A5), and (A6) to the recursive form of the Dyson equation

$$G^R=G^R_0+G^R_0\Sigma^R_{\mathrm{GW}}G^R_0+\cdots$$

and the Keldysh equation [53]

$$G^<=\big(1+G^R\Sigma^R_{\mathrm{GW}}\big)G^<_0\big(1+G^R\Sigma^R_{\mathrm{GW}}\big)^\dagger+G^R\Sigma^<_{\mathrm{GW}}G^{R\dagger},$$

we immediately get back to Eq. (A1) [68]. In the presence of disorder, the CPA iteration needs to be carried out as well. Using Eq. (A1) together with the equations in Sec. II B, one can easily verify that Σ_{CPA} follows the same relations as in Eqs. (A5) and (A6), providing that the impurity potential probability is an even function with respect to both the energy and the spatial position. Therefore, the relations in Eq. (A1) stay true throughout the self-consistent calculation. Now we can draw conclusion about how the drag current changes when $\mu^{(a)}$ is flipped:

$$\begin{aligned}I^{(p)}_{\mathcal{L}}(\mu^{(a)},\mu^{(p)})&=\int dE\,\mathrm{Tr}\big[G^{>(p)}(\mu^{(a)},\mu^{(p)})\Sigma^{<(p)}_{\mathcal{L}}\\&\quad-G^{<(p)}(\mu^{(a)},\mu^{(p)})\Sigma^{>(p)}_{\mathcal{L}}\big]\\&=\int dE\,\mathrm{Tr}\big[G^{>(p)}(-\mu^{(a)},\mu^{(p)})\Sigma^{<(p)}_{\mathcal{R}}\\&\quad-G^{<(p)}(-\mu^{(a)},\mu^{(p)})\Sigma^{>(p)}_{\mathcal{R}}\big]\\&=I^{(p)}_{\mathcal{R}}(-\mu^{(a)},\mu^{(p)})=-I^{(p)}_{\mathcal{L}}(-\mu^{(a)},\mu^{(p)}),\end{aligned}$$

where we have used the charge conservation law and the simple fact $\Sigma^{</>(p)}_{\mathcal{L},ij}(E)=\Sigma^{</>(p)}_{\mathcal{R},-i,-j}(E)$ due to the structural symmetry.

In the other situation where $\mu^{(a)}$ is fixed while $\mu^{(p)}$ is flipped instead, one can derive

$$G^{</>(p)}_{ij}(\mu^{(p)},E)=\eta_i\eta_j\big[G^{>/<(p)}_{ij}(-\mu^{(p)},-E)\big]^*,$$
$$\Sigma^{</>(p)}_{\mathcal{L},ij}(\mu^{(p)},E)=\eta_i\eta_j\big[\Sigma^{>/<(p)}_{\mathcal{L},ij}(-\mu^{(p)},-E)\big]^*,$$

and hence $J^{(p)}_{\mathcal{L}}(\mu^{(p)},E)=-J^{(p)}_{\mathcal{L}}(-\mu^{(p)},-E)$, which leads to $I^{(p)}_{\mathcal{L}}(\mu^{(a)},\mu^{(p)})=-I^{(p)}_{\mathcal{L}}(\mu^{(a)},-\mu^{(p)})$ upon being integrated over energy. This completes our analytic verification for the symmetry relation Eq. (11).

APPENDIX B: BAND STRUCTURE OF THE TIGHT-BINDING MODEL

In this Appendix, we present the noninteracting band structures of our tight-binding model with differing widths W (see Fig. 11).

[1] B. N. Narozhny and A. Levchenko, Rev. Mod. Phys. **88**, 025003 (2016).
[2] N. Giordano and J. D. Monnier, Phys. Rev. B **50**, 9363 (1994).
[3] T. J. Gramila, J. P. Eisenstein, A. H. MacDonald, L. N. Pfeiffer, and K. W. West, Phys. Rev. Lett. **66**, 1216 (1991).
[4] D. Laroche, G. Gervais, M. Lilly, and J. Reno, Nat. Nanotechnol. **6**, 793 (2011).
[5] D. Laroche, G. Gervais, M. Lilly, and J. Reno, Science **343**, 631 (2014).
[6] G. Shinkai, T. Hayashi, T. Ota, K. Muraki, and T. Fujisawa, Appl. Phys. Express **2**, 081101 (2009).
[7] D. Bischoff, M. Eich, O. Zilberberg, C. Rössler, T. Ihn, and K. Ensslin, Nano Lett. **15**, 6003 (2015).
[8] P. M. Solomon, P. J. Price, D. J. Frank, and D. C. La Tulipe, Phys. Rev. Lett. **63**, 2508 (1989).
[9] J.-D. Pillet, A. Cheng, T. Taniguchi, K. Watanabe, and P. Kim, arXiv:1612.05992v3.
[10] K. Flensberg, Ben Yu-Kuang Hu, A.-P. Jauho, and J. M. Kinaret, Phys. Rev. B **52**, 14761 (1995).
[11] A.-P. Jauho and H. Smith, Phys. Rev. B **47**, 4420 (1993).
[12] R. Sánchez, R. López, D. Sánchez, and M. Büttiker, Phys. Rev. Lett. **104**, 076801 (2010).
[13] A. Levchenko and A. Kamenev, Phys. Rev. Lett. **101**, 216806 (2008).
[14] A. Kamenev and Y. Oreg, Phys. Rev. B **52**, 7516 (1995).
[15] K. Lee, J. Xue, D. C. Dillen, K. Watanabe, T. Taniguchi, and E. Tutuc, Phys. Rev. Lett. **117**, 046803 (2016).
[16] M. Schütt, P. M. Ostrovsky, M. Titov, I. V. Gornyi, B. N. Narozhny, and A. D. Mirlin, Phys. Rev. Lett. **110**, 026601 (2013).

[17] J. C. W. Song and L. S. Levitov, Phys. Rev. Lett. **109**, 236602 (2012).
[18] K. Kaasbjerg and A.-P. Jauho, Phys. Rev. Lett. **116**, 196801 (2016).
[19] D. K. Efimkin and V. Galitski, Phys. Rev. Lett. **116**, 046801 (2016).
[20] S. S. Apostolov, A. Levchenko, and A. V. Andreev, Phys. Rev. B **89**, 121104 (2014).
[21] N. Kainaris, I. V. Gornyi, A. Levchenko, and D. G. Polyakov, Phys. Rev. B **95**, 045150 (2017).
[22] N. A. Mortensen, K. Flensberg, and A.-P. Jauho, Phys. Rev. B **65**, 085317 (2002).
[23] A. M. Lunde, K. Flensberg, and A.-P. Jauho, Phys. Rev. B **71**, 125408 (2005).
[24] X. F. Wang and I. C. da Cunha Lima, Phys. Rev. B **63**, 205312 (2001).
[25] P. Debray, V. Zverev, V. Gurevich, R. Klesse, and R. Newrock, Semicond. Sci. Technol. **17**, R21 (2002).
[26] V. L. Gurevich, V. B. Pevzner, and E. W. Fenton, J. Phys.: Condens. Matter **10**, 2551 (1998).
[27] O. Raichev and P. Vasilopoulos, Phys. Rev. B **61**, 7511 (2000).
[28] V. Moldoveanu, A. Manolescu, and V. Gudmundsson, Phys. Rev. B **82**, 085311 (2010).
[29] V. Moldoveanu and B. Tanatar, Europhys. Lett. **86**, 67004 (2009).
[30] B. L. Altshuler and A. G. Aronov, in *Electron-Electron Interactions in Disordered Systems*, Modern Problems in Condensed Matter Sciences, edited by A. L. Efros and M. Pollak (Elsevier, New York, 1985), Vol. 10, pp. 1–153.
[31] C. Zhou and H. Guo, Phys. Rev. B **95**, 035126 (2017).
[32] L. Zheng and A. H. MacDonald, Phys. Rev. B **48**, 8203 (1993).
[33] B. Tanatar and A. K. Das, Phys. Rev. B **61**, 15959 (2000).
[34] L. Hedin, Phys. Rev. **139**, A796 (1965).
[35] G. Onida, L. Reining, and A. Rubio, Rev. Mod. Phys. **74**, 601 (2002).
[36] I. Sodemann, D. A. Pesin, and A. H. MacDonald, Phys. Rev. B **85**, 195136 (2012).
[37] G. Baym and L. P. Kadanoff, Phys. Rev. **124**, 287 (1961).
[38] G. Baym, Phys. Rev. **127**, 1391 (1962).
[39] G. Stefanucci and R. Van Leeuwen, *Nonequilibrium Many-Body Theory of Quantum Systems: A Modern Introduction* (Cambridge University Press, Cambridge, 2013).
[40] P. Soven, Phys. Rev. **156**, 809 (1967).
[41] B. Velický, Phys. Rev. **184**, 614 (1969).
[42] Y. Kakehashi, Phys. Rev. B **66**, 104428 (2002).
[43] Y. Ke, K. Xia, and H. Guo, Phys. Rev. Lett. **100**, 166805 (2008).
[44] Y. Zhu, L. Liu, and H. Guo, Phys. Rev. B **88**, 205415 (2013).
[45] K. S. Thygesen and A. Rubio, Phys. Rev. B **77**, 115333 (2008).
[46] M. Strange, C. Rostgaard, H. Häkkinen, and K. S. Thygesen, Phys. Rev. B **83**, 115108 (2011).
[47] C. Jin and K. S. Thygesen, Phys. Rev. B **89**, 041102 (2014).
[48] Y. Ke, K. Xia, and H. Guo, Phys. Rev. Lett. **105**, 236801 (2010).
[49] Y. Zhu, L. Liu, and H. Guo, Phys. Rev. B **88**, 085420 (2013).
[50] D. Karlsson and C. Verdozzi, Phys. Rev. B **90**, 201109 (2014).
[51] Q. Shi, H. Guo, Y. Zhu, and L. Liu, Phys. Rev. Applied **3**, 064008 (2015).
[52] C. Zhou, X. Chen, and H. Guo, Phys. Rev. B **94**, 075426 (2016).
[53] H. Haug and A.-P. Jauho, *Quantum Kinetics in Transport and Optics of Semiconductors* (Springer, Berlin, 2008).
[54] M. L. Sancho, J. L. Sancho, J. L. Sancho, and J. Rubio, J. Phys. F **15**, 851 (1985).
[55] S. Datta, *Electronic Transport in Mesoscopic Systems* (Cambridge University Press, Cambridge, 1997).
[56] V. Moldoveanu and B. Tanatar, Phys. Rev. B **77**, 195302 (2008).
[57] W. H. Press, *Numerical Recipes: The Art of Scientific Computing*, 3rd ed. (Cambridge University Press, Cambridge, 2007).
[58] P. Pulay, Chem. Phys. Lett. **73**, 393 (1980).
[59] G. Kresse and J. Furthmüller, Comput. Mater. Sci. **6**, 15 (1996).
[60] N. A. Mortensen, K. Flensberg, and A.-P. Jauho, Phys. Rev. Lett. **86**, 1841 (2001).
[61] W.-K. Tse, Ben Yu-Kuang Hu, and S. Das Sarma, Phys. Rev. B **76**, 081401(R) (2007).
[62] L. E. Henrickson, A. J. Glick, G. W. Bryant, and D. F. Barbe, Phys. Rev. B **50**, 4482 (1994).
[63] A. P. Dmitriev, I. V. Gornyi, and D. G. Polyakov, Phys. Rev. B **86**, 245402 (2012).
[64] J. Taylor, H. Guo, and J. Wang, Phys. Rev. B **63**, 245407 (2001).
[65] K. Flensberg and Ben Yu-Kuang Hu, Phys. Rev. B **52**, 14796 (1995).
[66] R. Jalabert and S. Das Sarma, Phys. Rev. B **40**, 9723 (1989).
[67] J. Wang and H. Guo, Phys. Rev. B **79**, 045119 (2009).
[68] Taking the second term in the Dyson equation as an example, $G^{R(a)}_{0,ik}\Sigma^{R(a)}_{kl}G^{R(a)}_{0,lj}(\mu^{(a)},E)=[(-\eta_i\eta_k)G^{R(a)}_{0,-i,-k}(-\eta_k\eta_l)\Sigma^{R(a)}_{-k,-l}(-\eta_l\eta_j)G^{R(a)}_{0,-l,-j}(-\mu^{(a)},-E)]^*=(-\eta_i\eta_j)[G^{R(a)}_{0,-i,-k}\Sigma^{R(a)}_{-k,-l}G^{R(a)}_{0,-l,-j}(-\mu^{(a)},-E)]^*$. Repeated indices are summed over.